

Article

# Effect of Structure and Chemical Activation on the Adsorption Properties of Green Clay Minerals for the Removal of Cationic Dye

Abdelfattah Amari <sup>1,2,\*</sup>, Hatem Gannouni <sup>2</sup>, Mohammad I. Khan <sup>1</sup>, Mohammed K. Almesfer <sup>1</sup>,  
Abubakr M. Elkhaleefa <sup>1</sup> and Abdelaziz Gannouni <sup>2</sup>

<sup>1</sup> Department of Chemical Engineering, College of Engineering, King Khalid University, Abha 61421, Saudi Arabia; mkaan@kku.edu.sa (M.I.K.); almesfer@kku.edu.sa (M.K.A.); amelkhalee@kku.edu.sa (A.M.E.)

<sup>2</sup> R.U. Energy and Environment, National School of Engineers, Gabes University, Gabes 6072, Tunisia; hatgan@yahoo.com (H.G.); gannouniabdelaiz@yahoo.fr (A.G.)

\* Correspondence: aamary@kku.edu.sa

Received: 21 October 2018; Accepted: 13 November 2018; Published: 19 November 2018



**Abstract:** In this study, natural clay minerals with green appearance were treated with sulfuric acid. Mass percentage of acid (wt%), temperature (T), contact time (t) and liquid-to-solid mass ratio (R) are used as the prevailing factors that determine the extent of acid-activation. The values of these factors range from 15–50%, 60–90 °C, 1.5–6 h and 4–7, respectively. The study has focused on the structural changes as well as textural characteristics of the clay. Three activated clay samples were prepared under different treatment conditions. The samples were characterized using X-ray powder diffraction (XRD), fourier transform infrared (FTIR), scanning electron microscope (SEM), chemical analysis and N<sub>2</sub> adsorption techniques. Characterization of the treated clay minerals exhibited significant structural changes to a greater extent of acid-activation, from being partially crystalline to being amorphous silica. The surface area and total pore volume of clay increased proportionally with the level of acid treatment. The average pore diameter behaved differently. During the strong acid treatment, a large increase in pore volume and the enlargement of the pore size distribution were observed. This suggests that considerable structural changes and partial destruction may have occurred in this condition. The removal of methylene blue, used as cationic dye, from aqueous solution by the batch adsorption technique on three prepared acid-activated clay samples was studied. The Langmuir model was found to agree well with the experimental data.

**Keywords:** clay minerals; acid activation; characterization; structural changes; cationic dye; adsorption

## 1. Introduction

Clays and clay minerals are of significant interest because of their interesting characteristics that make them suitable for industrial applications. They have been accepted as one of the most appropriate low-cost adsorbents and common component in different industrial applications [1–7]. Among the various types of clays, bentonite is more popular. Its physicochemical and adsorption properties depend on the montmorillonite content, the crystalline structure of the clay minerals that constitute them and the nature of the inter-layer cations [8,9]. In order to eliminate impurities and different exchangeable cations from clay minerals and to prepare a well-defined material for use as catalyst and adsorbent, various activations have been used, most often with inorganic acids [10–13]. Indeed, the treatment with minerals acids significantly changed their textural characteristics. This can expand their applications to include environmental protection [14,15], catalytic cracking of petroleum [16], catalyst supports in many chemical processes and detergent

in paper industries and textile fabrications [17–19]. In fact, the most applications of these clays are bleaching, purification and stabilization of vegetable oils.

Acid-activated clays have attracted much current interest as adsorbents and catalysts for a range of acid mediated processes [20–22]. Nowadays, considerable progress is achieved in the synthesis of many new inorganic mesoporous molecular sieves based on solid acids. However, modified clay minerals remain one of the widely and mostly used in the industry as mesoporous solid catalysts and adsorbents [23]. The acid attack on clay minerals has additional effects on the mineralogical composition of the raw material and related properties; that is, organic matter is leached out and feldspar can be partly attacked (or dissolved). This process causes increase in surface area and surface acidity and introduces permanent mesoporosity [18,24–27] and also removes metal ions from the crystal interlayer, which partially delaminated the clay.

The acid treatment strips octahedral ions such as Fe, Al, Mg and removes tetrahedral ions from the clay minerals due to the isomorphous substitution in the crystal lattices [28]. The extent to which these ions are removed depends on the relevant factors. Several factors may contribute when a clay undergoes an acid activation such as; the nature of acid, the mass percentage of acid, the temperature of activation reaction, contact time of solid-to-liquid, the stirring rate of mixture, the size of the solid particle and the liquid-to-solid mass ratio. Four parameters are known to strongly influence the structural properties and can affect significantly the required results: the temperature, the contact time, the solid-to-liquid ratio and mass percentage of acid. These parameters are the main factors that delimit the extent of acid-activation and thus, the induced physicochemical and structural changes [13–15]. As a consequence of these structural changes, acid-treatment can extend the fields of application of these porous solids such as in the control of atmospheric pollution [15]. This work is a continuation of numerous studies carried out in the field of surface and colloid science and dealing with clay minerals [15,29–35]. Natural green clay mineral collected from south of Tunisia was treated with sulfuric acid in order to prepare suitable adsorbent for several organic compounds. The present work aims to prepare, characterize and investigate the effect of acid treatment factors on some physicochemical and bleaching properties of the raw material. Removal of cationic dye, methylene blue used as textile dye in industries, by the batch adsorption technique was studied.

## 2. Materials and Methods

### 2.1. Materials

All the required chemicals used in this work were of analytical grade. Sulfuric acid  $H_2SO_4$  and Methylene blue (MB) were purchased from Sigma-Aldrich chemicals (Saint Louis, MO, USA). The formula of MB is  $C_{16}H_{18}N_3S^+Cl^- \cdot 2H_2O$ , the molecule is positively charged and its aromatic moiety is planar.

A MB stock solution of mass concentration 1 g/L was prepared by dissolving 1 g of dye in double distilled water in 1000 mL volumetric flask. Other required solutions with various dye concentrations in the range of 10 mg/L to 120 mg/L, were prepared by serial dilution. The pH of solutions was adjusted using 0.1 M solution of HCl or NaOH. The structural formula of methylene blue is given in Figure 1.

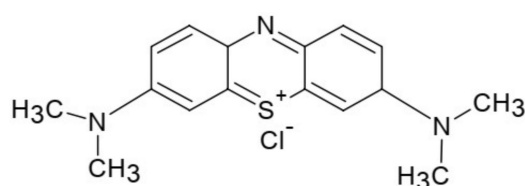


Figure 1. Structure of methylene blue.

## 2.2. Adsorption Studies

In this section, batch adsorption technique is used. Appropriate clay quantity of 200 mg was added in 250 mL conical flask to solutions of MB of different initial concentrations and stirred by magnetic hot plate stirrer with 10 positions of model MS-H-S10 (Scilogex, Rocky Hill, NJ, USA) at the rate 300 rpm and at temperature 20 °C. The time required to attain equilibrium was predetermined previously based on some experiments of kinetic study and estimated to be 60 min. To ensure that the time chosen was enough to reach equilibrium, all experiments were conducted at 1.5 h. Once the dye solutions had reached equilibrium, the suspensions were separated by centrifugation within 30 min at the rate of 3000 rpm using centrifuge of type 80-2C (Xiangtian, Jiangsu, China), for further analysis of the dye concentrations. The residual concentration of the dyes was determined using a UV-visible spectrophotometer of model UV-1700 (Shimadzu corporation, Kyoto, Japan) at 665 nm. The pH of the solutions for adsorption experiments was set to 7 and controlled using a pH-Meter of type Basic 20+ (Crison instruments, Barcelona, Spain). The temperature of experiments was maintained at 20 °C and its control was performed using a thermostatically controlled incubator.

The amount of MB adsorbed  $q_e$  (mg/g) was calculated from the difference between the initial and equilibrium MB concentrations and is given by:

$$q_e = \frac{(C_0 - C_e) \times V}{m}$$

$C_e$  (mg/L) is the concentration of adsorbate at equilibrium;  $C_0$  (mg/L) is the initial concentration of adsorbate;  $m$  (g) is the mass of the adsorbent; and  $V$  (L) is the volume of the solution.

## 2.3. Preparation and Purification of the Adsorbent

The starting material is clay collected from the deposit of “Djebel Aïdoudi” of “Hamma,” located in south Tunisia, at the east of Gabes town. The raw material contained, in addition to the mineral phases, impurities which can be reduced or eliminated completely by applying a purification protocol. After collection and before use for activation, the raw material is purified by sedimentation. This is achieved by suspending the crude lumps in distilled water at mass ratio 1:10 (clay:water). The mixture was stirred very vigorously to ensure efficient mixing and then sieving was carried out three times through a sieve of different mesh size and particles smaller than 43 µm were collected. Then, the suspended particles were recovered after allowing coarser mineral particles to settle. Finally, the water is siphoned off and the clay is dried in an air oven at 60 °C.

## 2.4. Preparation and Analysis of Oriented Aggregates of Clay

Oriented aggregate specimens of clay were carried out using the standard procedure of Brown and Brindley [33] according to the following steps [36]: a few gram of finely ground clay was added to a vessel containing distilled water and then the mixture was stirred and allowed to stand. After a few minutes, the heavy and/or coarse fractions are separated by decanting. Only clay grains that remain suspended in the liquid are removed using a pipette. The liquid was extended on a horizontal glass slide to obtain a well oriented regular deposit, then left to dry in open air. Three oriented clay specimens were prepared; the first one was analyzed in normal state. The normal state of the material refers to the raw material, merely freed from its coarse fraction by sedimentation and keeping the clay fraction in its natural state (without changing the interlayer space by ion exchange). This sample was used as the reference to judge the movements caused by other treatments. The second one is subjected to ethylene glycol vapor in a desiccator for 24 h (glycolated aggregate), this treatment leads to the swelling of smectites. The last one is heated in an oven for one hour at a temperature of 500 °C. This heating can destroy kaolinite and keep chlorite. After this treatment, the minerals of smectite group are dehydrated irreversibly and interlayer space will be blocked to 10 Å.

### 2.5. Acid Activation of Raw Material

Clay mineral was treated with sulfuric acid. According to previous works [12] and preliminary tests, it was shown that the particle size of the solid had no significant effect on the kinetics of the activation or the pore properties of clay particles when the dimensions were equal to or less than 40  $\mu\text{m}$ . Moreover, it was found that the agitation does not have much effect on the kinetics of the acid attack from certain values. Hence, the stirring has been adjusted to the maximum value of a laboratory stirrer in order to ensure the homogenization of the reaction mixture. Consequently, this study was conducted using only four major factors: the strength of acid (wt%), the reaction temperature (T), the reaction time (t) and the liquid to solid mass ratio (R).

Based on preliminary tests and from the literature review [12], samples were prepared according to the following ranges: Temperature (60–90  $^{\circ}\text{C}$ ), contact time (1.5–6 h), liquid/solid mass ratio (4–7) and mass percentage of acid (15–50%). It was shown that the selected ranges of these factors, are appropriate to investigate the effect of acid activation on raw material and efficient to make difference in activation degree between the samples. Three activated clay samples were prepared: the first sample ( $S_1$ ) was prepared under low conditions (wt = 15%, T = 60  $^{\circ}\text{C}$ , t = 1.5 h, R = 4), the second sample ( $S_2$ ) was activated at average conditions (wt = 32.5%, T = 75  $^{\circ}\text{C}$ , t = 3.75 h, R = 5.5), while the last sample ( $S_3$ ) was prepared under strong conditions (wt = 50%, T = 90  $^{\circ}\text{C}$ , t = 6 h, R = 7).

A series of treatment steps were used for the acid-treatment of clay. Experiments were carried out with sulfuric acid in a jacketed glass reactor equipped with a thermometer, a reflux condenser and a stirrer. Each sample was prepared according to the following procedure: 100 g of raw clay, with a particle size less than 40  $\mu\text{m}$ , was mixed with an appropriate aqueous solution of  $\text{H}_2\text{SO}_4$ . The slurry was stirred at maximum speed by a laboratory agitator of type Kirk 210 (Bicasa, Monza Brianza, Italy). Then, slurry was air-cooled and filtered with a glass fibber. The filter cake was washed with distilled water several times until the wash water was neutral with no trace of sulphate. The pH of the filtrate is monitored by universal pH test strips.

Finally, the clay product was dried in an oven at 70  $^{\circ}\text{C}$  for 48 h until the weight remains constant. The freshly prepared dry sample was crushed into powder by a mortar. Then the activated clay was sieved before use according to U.S. standard sieve designations (Afnor nF-11504). All the activated clay samples ( $S_1$ ,  $S_2$  and  $S_3$ ) were prepared with the same described procedure.

### 3. Characterization

The mineralogical compositions were determined by the techniques of X-ray powder diffraction (XRD) using Philips Panalytical X' Pert PRO powder diffractometer (Almelo, The Netherlands) equipped with X' Celerator detector and with cobalt  $K_{\alpha}$  radiation ( $\lambda = 1.789 \text{ \AA}$ ). Tension and current were set to 40 kV and 40 mA respectively. Scans were collected between 3 and 60 $^{\circ}$  2 $\theta$  angular range at steep angle of 0.017 $^{\circ}$ . Orientated aggregate samples were scanned from 3 $^{\circ}$  to 35 $^{\circ}$  2 $\theta$  angular range at 1 $^{\circ}$ /min with a scanning step of 0.01 $^{\circ}$ /step. The clay fraction was maintained at three different conditions (1 to 3); 1: untreated (natural state), 2: after treatment with ethylene glycol vapors in a desiccator for 24 h at 60  $^{\circ}\text{C}$ , 3: after heating at 500  $^{\circ}\text{C}$  for 1 h. The micromorphological features of the samples before and after activation were studied using a scanning electron microscope (SEM) of type Philips XL30 ESEM (Leuven, Belgium) operating with up to 30 kV acceleration voltage field emission gun. Sample clays fragments were previously coated with a thin layer of gold before proceeding to morphological observations. The Fourier transform infrared spectroscopy (FT-IR) was applied using a Perkin-Elmer 983 G IR-spectrometer (Bridgeport, CT, USA) equipped with IR source, KBr beam splitter and DTGS KBr detector. Prior to analysis, samples were lightly ground using a mortar and pestle and sieved again through the 45  $\mu\text{m}$  sieve. This was done to minimize the scattering, distortion and peak broadening of IR radiation due to larger-sized particles that may have resulted from agglomeration during drying. The spectra were recorded in the spectral range from 4000 to 250  $\text{cm}^{-1}$ . Quantitative chemical analysis of raw material ( $S_0$ ) and acid-activated clays were performed using atomic absorption spectrometer (AAS) of type NOVAA 400 (Analytik Jena AG, Jena, Germany)

and X-ray fluorescence (ARL<sup>®</sup> 9800 XP spectrometer, Thermo ARL, Ecublens, Switzerland). By X-ray fluorescence, the loss on ignition (LOI) content of dried and powdered clay sample was attributed to the release of water and was measured by calcinations at 975 °C. Then the dried clay samples were mixed with lithium-tetraborate and lithium iodide and the mixture was fused in a Pt crucible and moulded to a glass disk for chemical analysis. N<sub>2</sub> adsorption/desorption isotherms were measured using Quantachrome Autosorb AS1C (Quantachrome Instruments, Boynton Beach, FL, USA) equipment at liquid nitrogen temperature of −196.15 °C. Before adsorption measurements, the samples were degassed in vacuum at 300 °C for more than 3 h to remove any adsorbed contaminants from the surface and pores of the samples. The Brunauer-Emmett-Teller (BET) method was used to determine the surface areas and pore volume of samples and the pore size distribution was calculated using the BJH method based on the nitrogen adsorption or desorption data.

#### 4. Results and Discussions

After acid-activation, clays underwent chemical analysis and textural characterizations. The expected results obtained by acid-activated clays ( $S_1$ ,  $S_2$ ,  $S_3$ ) were compared to those found by raw material ( $S_0$ ). For full description of the mineralogical composition of clay materials and to understand the structure changes, it is required first to determine the nature of the various impurities contained in each sample. The reflections of phyllic phases were then established.

##### 4.1. Determination of Non-Clay Minerals

It should be noted that the quantification of non-clay minerals found in the clays by XRD alone was difficult, since some components are hardly detectable by X-ray. These non-clay minerals in the raw material were marked by different peaks. An X-ray diffraction pattern of raw clay mineral ( $S_0$ ) is shown in Figure 2.

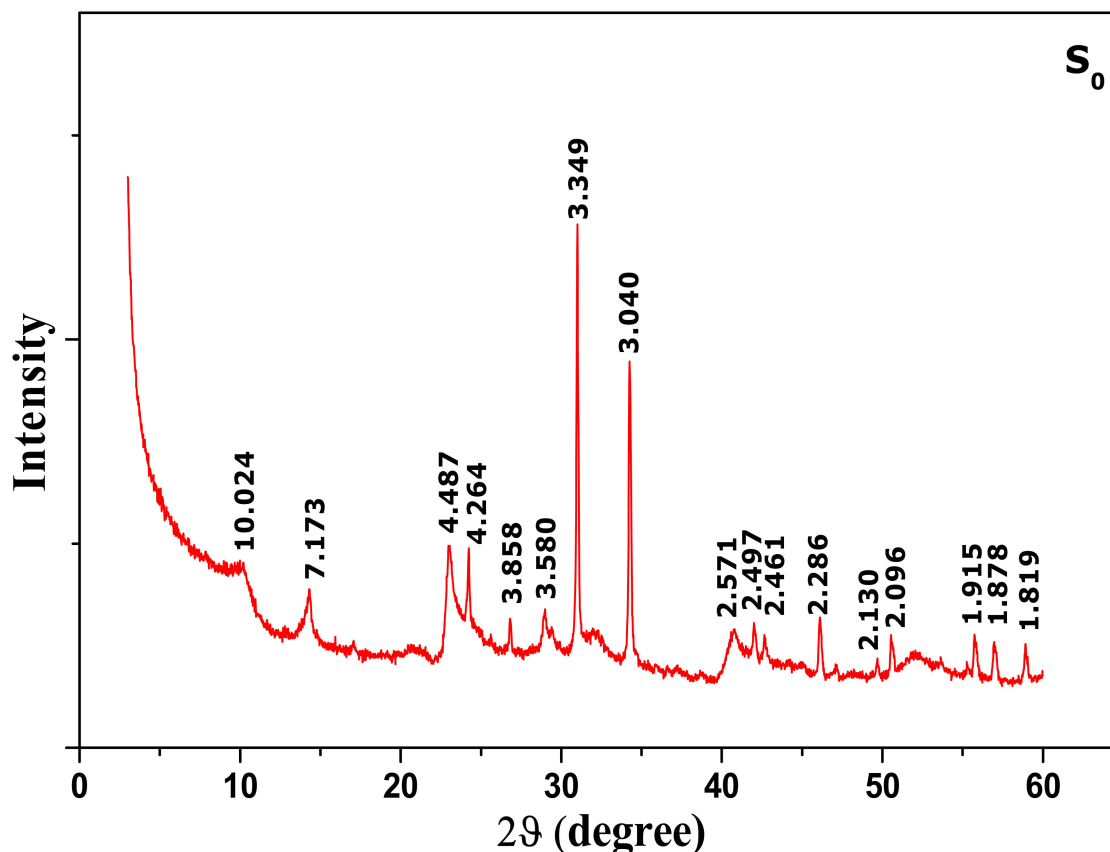
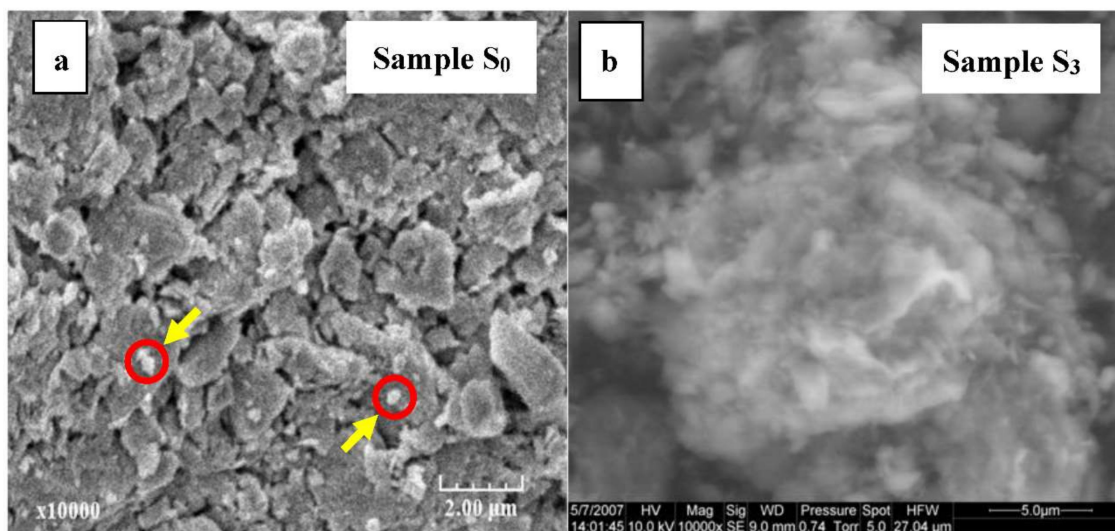


Figure 2. X-ray diffraction (XRD) patterns of raw material ( $S_0$ ).

Quartz appeared as major non-clay minerals by the reflection peaks observed at  $d = 3.34$ ;  $2.28$ ;  $2.13$ ;  $1.819$  Å and  $d = 4.26$  Å. Other non-clay minerals are also detected, such as the calcite at  $3.858$ ;  $3.04$ ;  $1.915$ ,  $1.878$  Å and gypsum at  $2.09$  Å. It is remarkable that the non-clay minerals were still present even after purification. This is probably due to their fine particle size which makes their complete separation impossible during clay pre-treatment.

#### 4.2. Observation by Scanning Electron Microscope (SEM)

Figure 3 presents the morphologies of raw material ( $S_0$ ) and the acid-activated clay prepared at strong condition ( $S_3$ ) observed by SEM.



**Figure 3.** Scanning electronic micrographs of raw material  $S_0$  (a) and acid-activated clay sample  $S_3$  (b).

In agreement with the results obtained from XRD patterns, very large aggregates appeared on SEM images of the raw material (Figure 3a) (size up to 400 nm approximately) and well observed deposited on the mineral layers (indicated by an arrow). These minerals of small size, considered as non-clay minerals, are closely associated to clay and not easily eliminated during purification. Also, SEM examination revealed natural clay morphology of very fine-grained aggregates of clay platelets, irregular curved flakes and mats of coalesced flakes. In any case and because of particle coalescence, it is difficult to determine their exact texture. A sharp decrease in particle size caused by acid activation is visible in the modified clay (Figure 3b). It consists mainly of small aggregates of nanoparticles and exhibits a distinct porous structure.

#### 4.3. Determination of the Phyllic Phases by X-ray Diffraction

The XRD patterns of oriented specimens, natural state (air dried), saturated with ethylene glycol and heated at 500 °C of raw clay sample,  $S_0$ , are illustrated in Figure 4.

A non-symmetrical peak at 15.05 Å is observed by X-ray diffraction patterns of (001) reflection for the air-dried sample. This peak is characteristic of divalent cations occupying the interlayer sites. Once the sample is saturated by ethylene glycol, the peak expands to 17.39 Å, indicating the presence of smectite. This phase of expandable layers remain predominant. The asymmetrical form of the latter reflection is characteristic of a partly interstratified phase illite/smectite. It is frequently observed that illite is interstratified with the smectite by small particles included in the smectite [34,35]. It is not ambiguous that the reflections at 7.18 Å and 3.58 Å unaffected by the treatment with ethylene glycol and disappeared following the heat treatment, correspond to the reflection of the phyllic phase 1:1 kaolinite. As previously mentioned, the examination of oriented clay specimens by X-ray

diffraction shows peaks at 3.34 Å and 3.03 Å corresponding to quartz and calcite, respectively. The infrared spectrum (IR) of natural clay ( $S_0$ ) is presented in Figure 5.

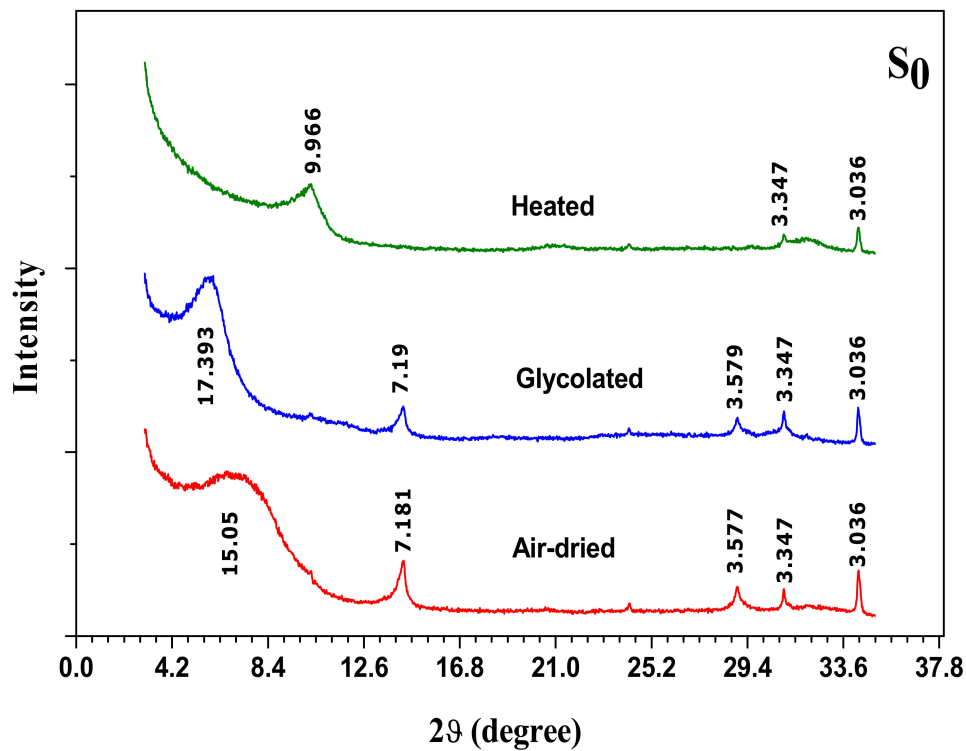


Figure 4. XRD patterns of oriented aggregate specimens of raw material ( $S_0$ ): Air dried, glycolated and heated to 500 °C.

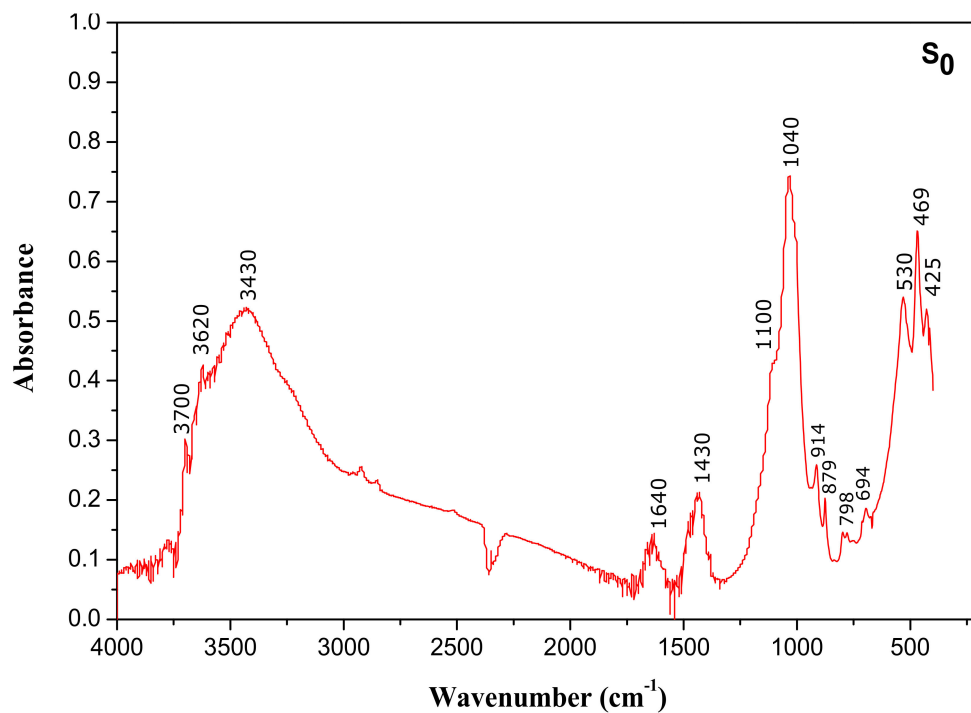


Figure 5. Fourier transform infrared (FTIR) spectrum of raw material ( $S_0$ ).

The results of IR spectrum (Figure 5) confirmed the data obtained by X-ray diffraction, that is, smectite was the dominant mineral phase. The two bands between  $3500\text{ cm}^{-1}$  and  $3700\text{ cm}^{-1}$  and near  $3430\text{ cm}^{-1}$  indicate the presence of smectite [35]. The peak at  $3620\text{ cm}^{-1}$  is assigned to stretching vibrations of the OH group of water molecules. The broad band at  $3430\text{ cm}^{-1}$  and the band at  $1640\text{ cm}^{-1}$  belong to the OH stretching and bending vibration of sorbed water molecules present in the clay, respectively. Furthermore, the strong absorption band at  $1040\text{ cm}^{-1}$  and the band at  $795\text{ cm}^{-1}$  are a result of Si–O stretching vibrations, whereas the bands at  $528$  and  $472\text{ cm}^{-1}$  are assigned to the deformation vibrations of Si–O–Al and Si–O–Si, respectively.

#### 4.4. Effect of Acid-Activation

Changes in crystallinity resulting from acid activation of raw material were investigated by the X-ray powder diffraction patterns of some typical samples. Figure 6 presents the XRD patterns together of raw material  $S_0$  and acid-activated clays ( $S_1, S_2, S_3$ ).

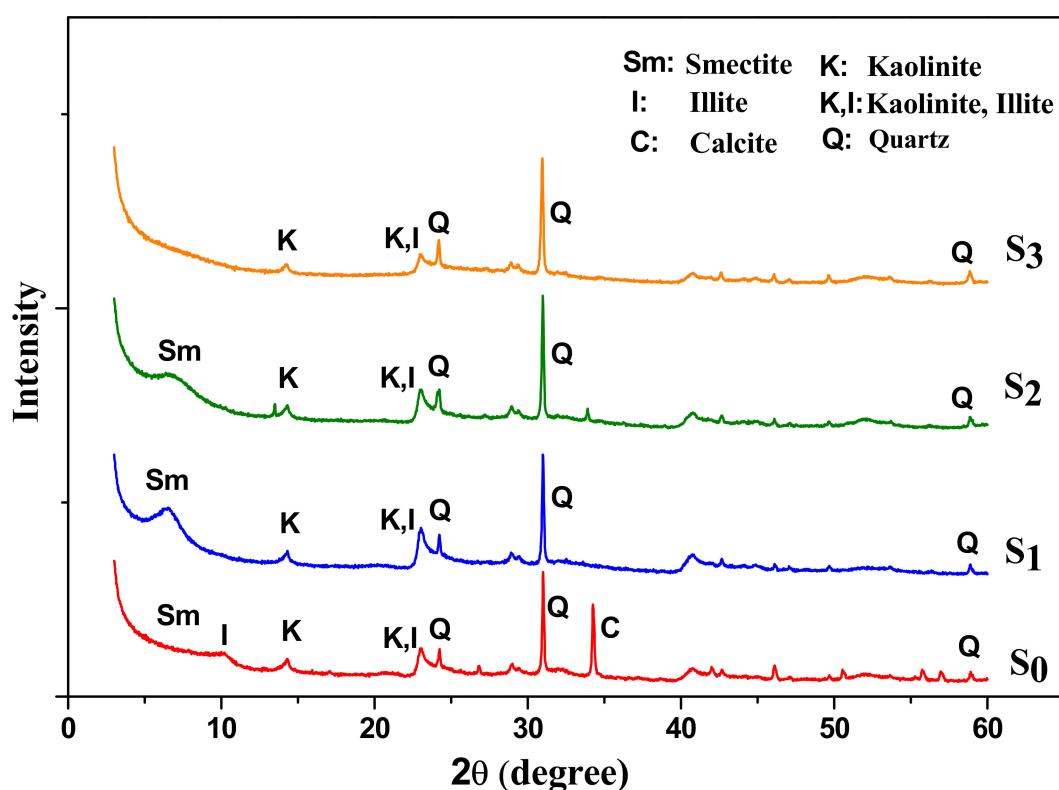


Figure 6. XRD patterns of raw material ( $S_0$ ) and acid-activated clay samples ( $S_1, S_2, S_3$ ).

The pattern of raw material is shown here for sake of comparison. It is observed that acid-activation causes a clear decrease in the crystallinity as indicated by decreasing intensity of the smectite peaks. Some of them are gradually deteriorated and completely disappeared. As it can be seen, XRD analysis has shown that clay acid-activation leads to total dissolution of calcite (reflections at  $3.858; 3.04; 1.915$  and  $1.878\text{ \AA}$ ) and gypsum (reflections at  $2.09\text{ \AA}$ ).

Under strong conditions of  $\text{H}_2\text{SO}_4$ , some of the quartz peaks are still present in the activated samples indicating that quartz is more resistant to acid attack than smectite. This result was similar to that found by Komadel and Madejova [13], hence quartz which appeared as the most abundant non-clay mineral in the natural clay (see reflections at  $d = 3.34; 2.28; 2.13; 1.819\text{ \AA}$  and  $d = 4.26\text{ \AA}$ ) cannot be completely eliminated from clay by acid-activation. Temuujin et al. [36] have reported similar results for montmorillonite activated by hydrochloric acid. For a greater extent of acid treatment (sample  $S_3$ ), it is observed that layered structure of clay mineral is indicated by the loss of crystallinity

and the appearance of amorphous silica remaining from leached smectite phase. These results are in agreement with those obtained by Shinoda et al. [37]; indicating that the acid-activated product of smectite is generally amorphous silica.

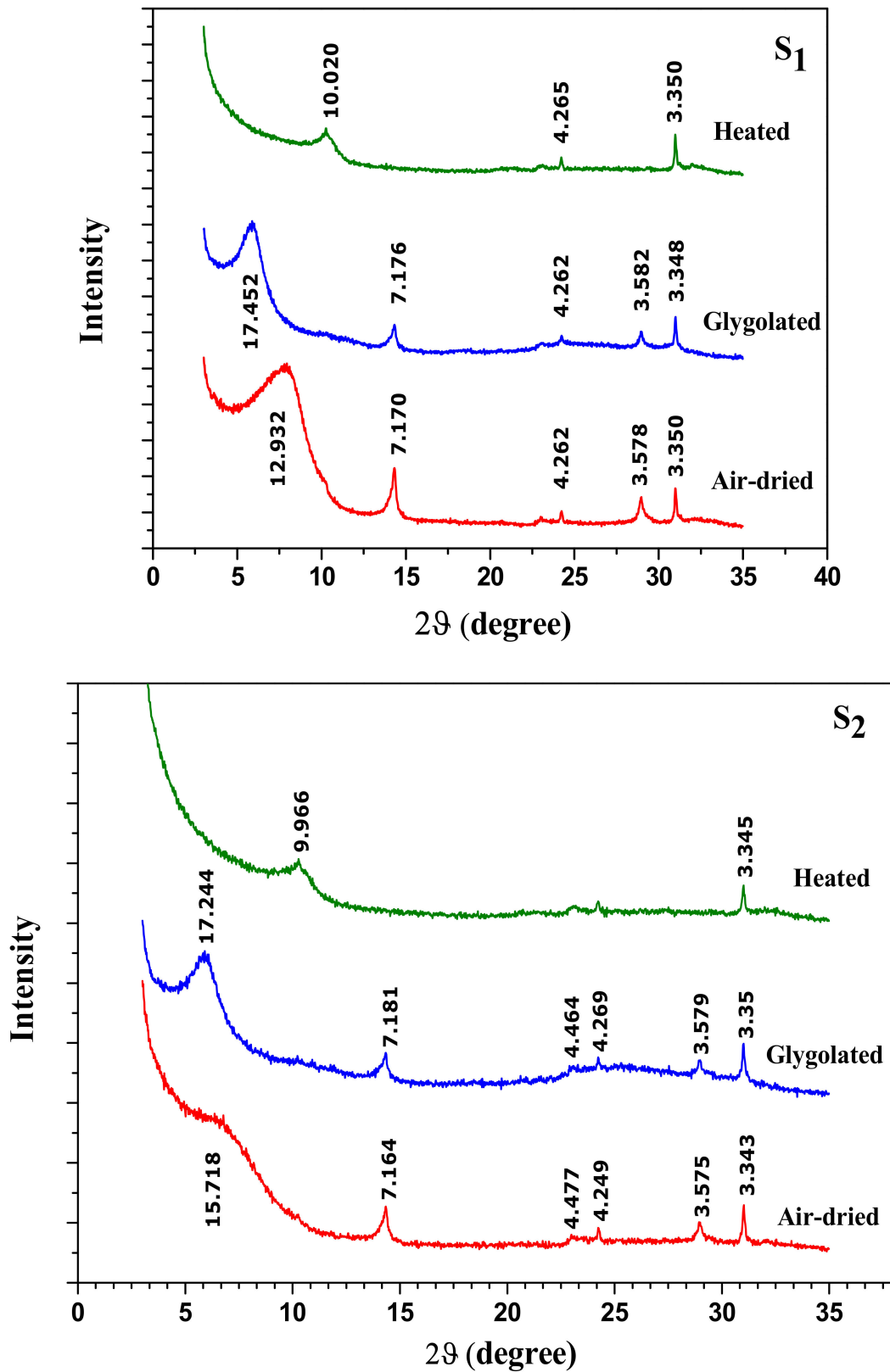
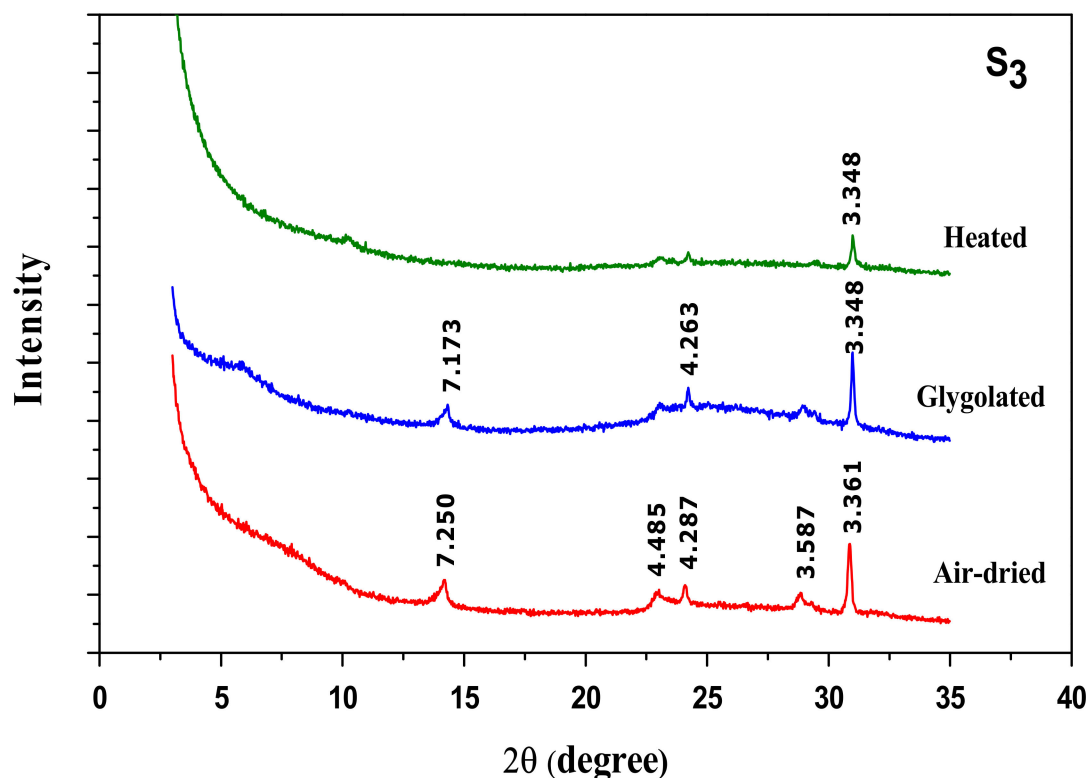


Figure 7. Cont.



**Figure 7.** XRD patterns of oriented activated clay specimens prepared under different conditions:  $S_1$  (low conditions),  $S_2$  (average conditions) and  $S_3$  (strong conditions).

X-ray diffraction patterns of oriented activated clay specimens (Figure 7  $S_1$ – $S_3$ ) prove a complete disappearance of the interstratified phase illite/smectite for the severity conditions but no effect on the kaolinite phase was observed (reflection at  $d = 7.18 \text{ \AA}$  and  $d = 3.58 \text{ \AA}$ ).

From these results, it can be concluded that acid treatment mainly affected the smectite phase and led to a partial decrystallization of the clay structure.

The IR spectra presented in Figure 8 showed that the acid-activation led to a partial dissolution of the octahedral sheets especially with the sample  $S_3$  prepared at high conditions of acid treatment. This is confirmed by the decrease in intensity of the band at  $914 \text{ cm}^{-1}$  corresponding to  $-\text{OH}$  bending vibration ( $\text{AlAlOH}$ ), bands at  $530 \text{ cm}^{-1}$  assigned to  $(\text{Si}-\text{O}-\text{Al})$ ,  $1030 \text{ cm}^{-1}$  attributed to  $(\text{Si}-\text{O})$  and band at  $3430 \text{ cm}^{-1}$  related to adsorbed  $\text{H}_2\text{O}$ . The broadening of the IR bands between  $1100$  and  $900 \text{ cm}^{-1}$  is indicative of the formation of amorphous opal.

In addition, a significant decrease or almost disappearance of the band at  $3620 \text{ cm}^{-1}$  was observed, this is due to the important leaching of cations after the acid activation. The comparison between raw material and acid-activated clay IR spectra showed that for more severe conditions ( $S_3$ ), acid-activation destroys the smectite mineral phase as proved by the disappearance of the bands located between  $3500 \text{ cm}^{-1}$  and  $3700 \text{ cm}^{-1}$  [35]. The complete disappearance of bands at  $1430 \text{ cm}^{-1}$  and  $872 \text{ cm}^{-1}$  pointed out to the dissolution of calcite  $\text{CaCO}_3$  and dolomite  $\text{CaMg}(\text{CO}_3)$  for the three samples ( $S_1$ ,  $S_2$ ,  $S_3$ ) as previously reported by Khalil et al. [38].

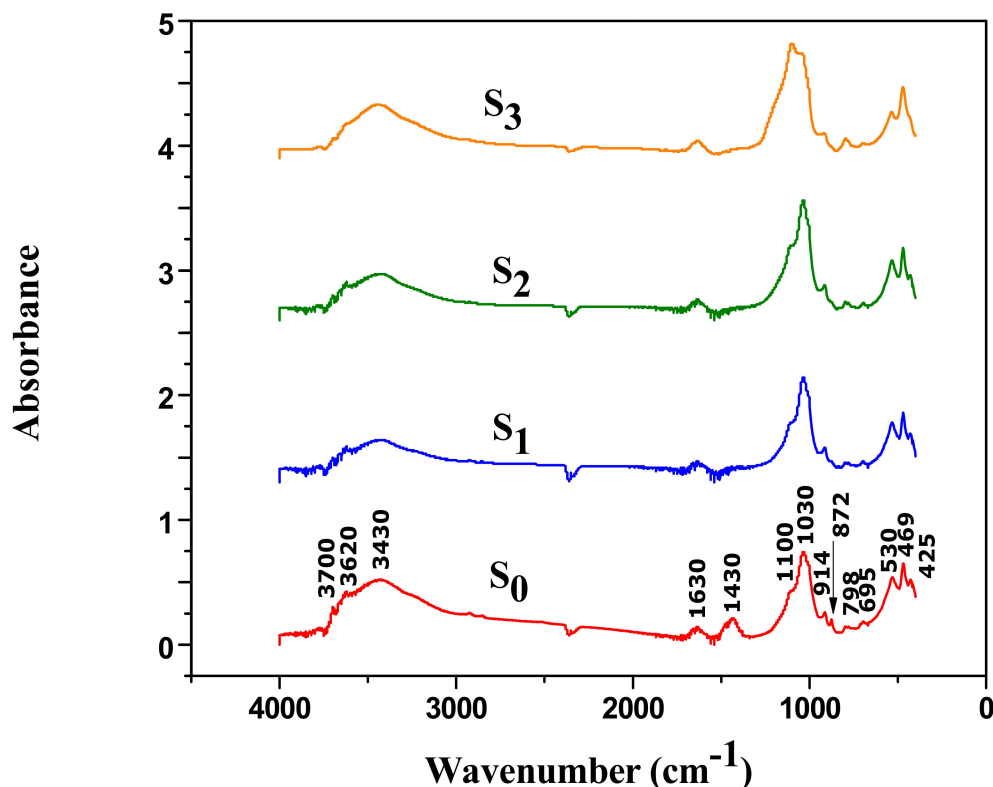


Figure 8. Infra-red spectra of raw material ( $S_0$ ) and acid-activated clays ( $S_1$ ,  $S_2$ ,  $S_3$ ).

Chemical analysis was performed on both raw material ( $S_0$ ) and acidified clays ( $S_1$ ,  $S_2$  and  $S_3$ ). The results are illustrated in Table 1.

Table 1. Chemical analyses of raw material ( $S_0$ ) and acid activated clay samples ( $S_1$ ,  $S_2$ ,  $S_3$ ).

Samples	MgO	Fe <sub>2</sub> O <sub>3</sub>	Al <sub>2</sub> O <sub>3</sub>	SiO <sub>2</sub>	SO <sub>3</sub>	CaO	K <sub>2</sub> O	Na <sub>2</sub> O	P <sub>2</sub> O <sub>5</sub>	TiO <sub>2</sub>	ZnO	L.I. at 975 °C
$S_0$	1.46	6.07	14.27	49.87	0.77	7.00	1.09	0.53	0.19	1.41	0.18	17.62
$S_1$	1.23	5.56	13.58	50.82	0.76	0.86	1.03	0.23	0.06	1.62	0.37	16.54
$S_2$	0.98	4.89	12.38	52.69	0.75	0.58	0.97	0.11	0.01	1.80	0.51	15.27
$S_3$	0.43	1.89	9.40	67.63	0.68	0.14	0.61	0.13	0.01	2.26	0.24	11.24

L.I. Loss on Ignition.

The chemical analysis of raw clay ( $S_0$ ) proved the presence of silica, alumina, iron and calcium as major constituents, along with traces of sodium, potassium, phosphate and titanium oxides. The higher mass percentage of silica and alumina reveals that clay mineral is an aluminosilicate matter.

After acid-activation, the SiO<sub>2</sub> content of clay ( $S_0$ ) increased from 49.87% to 50.82%, 52.69% and 67.63% for  $S_1$ ,  $S_2$  and  $S_3$ , respectively. However the content of Al<sub>2</sub>O<sub>3</sub>, Fe<sub>2</sub>O<sub>3</sub> and MgO are decreased from 14.27%, 6.07% and 1.46% to 13.58%, 5.56%, 1.23% and to 12.38%, 4.89%, 0.98% and to 9.4%, 1.89%, 0.43%, for  $S_1$ ,  $S_2$  and  $S_3$ , respectively. This may be due to the partial destruction (dissolution) of the octahedral layer (Al,Fe,Mg–O layers) and the exposure of the tetrahedral layers (Si–O layers) in acid solution.

The N<sub>2</sub> adsorption/desorption isotherms of raw material and activated clays presented in Figure 9 showed that isotherms are reversible for lower equilibrium pressure but at higher relative pressure, they exhibited a hysteresis loop of H<sub>3</sub> type [39]. Such hysteresis loops exist in the slit-shaped pores or in the ink-bottle pores (pores with narrow necks and wide bodies).

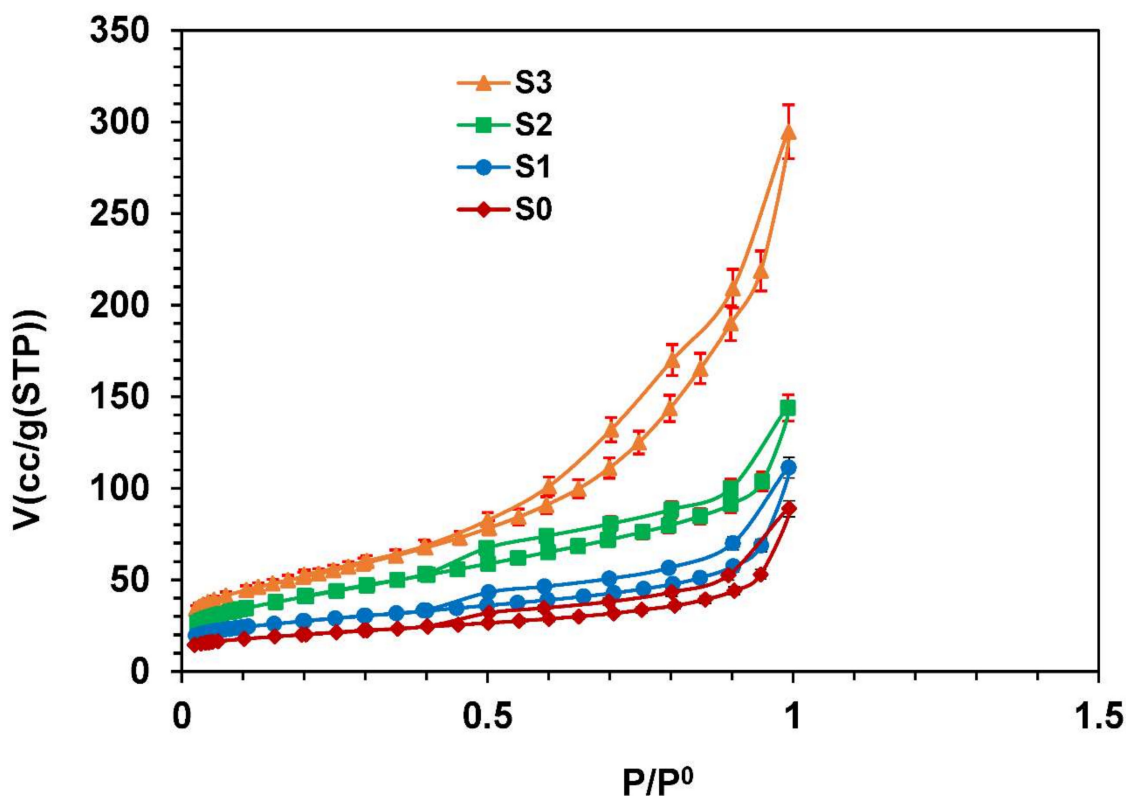


**Figure 9.** N<sub>2</sub> adsorption isotherms of the raw material (S<sub>0</sub>) and activated clay samples (S<sub>1</sub>, S<sub>2</sub>, S<sub>3</sub>) with ±5% error bars in volume.

The textural properties of raw clay (S<sub>0</sub>) and acid-activated clays (S<sub>1</sub>, S<sub>2</sub>, S<sub>3</sub>) are presented in Table 2.

**Table 2.** Textural properties of raw material (S<sub>0</sub>) and acid-activated clay samples (S<sub>1</sub>, S<sub>2</sub>, S<sub>3</sub>).

Samples	Total Pore Volume (10 <sup>-2</sup> cm <sup>3</sup> /g)	Average Pore Diameter (Å)	BET Surface Area. S <sub>BET</sub> (m <sup>2</sup> /g)
S <sub>0</sub>	13.74	79.56	69.00
S <sub>1</sub>	17.20	72.92	94.36
S <sub>2</sub>	22.26	60.76	146.50
S <sub>3</sub>	45.58	98.9	184.40

It can be noted that surface area, total pore volume and average pore diameter were changed as the severity of acid treatment was increased. Data presented in Table 2 shows that surface area depends on acid attack but the relation between surface area and acid treatment is non-linear. Taylor et al. have reported that surface area increases with acid concentration [25]. As it can be seen from Table 2, acid activation improves the volume of pores. The pore volume was only 0.1374 cm<sup>3</sup>/g for natural clay (S<sub>0</sub>) but after acid treatment it becomes much higher and reaches 0.4558 cm<sup>3</sup>/g for more severe treatment (sample S<sub>3</sub>). Assuming that the pores are cylindrical, the mean pore diameter was calculated from the formula  $d = 4V_p/S_p$ . where,  $V_p$  is the pore volume and  $S_p$  is the specific surface area of the pores. The average pore diameter for starting material (S<sub>0</sub>) is 79.56 Å. It decreases for low acid treatment and average condition and then increases at higher conditions for sample S<sub>3</sub>, to reach the value of 98.9 Å. This can be explained by the fact that acid-activated samples had a greater increase in percentage of pore volume of micro pores than meso pores. As a consequence the lower values of the average pore diameter for samples S<sub>1</sub> and S<sub>2</sub> were obtained compared to that of natural clay. However, the strong acid treatment that produced S<sub>3</sub>, caused large increase of pore volume in the range of micro pore and meso pore diameter and consequently an increase in average pore

diameter. This suggests a considerable structural changes and decomposition occurred in this sample. A similar result was observed by Jovanovic and Janackovic [40].

The change in mean pore diameter with the acid treatment is also confirmed by the mesopore size distribution curve calculated by BJH equation [41]. The pore size distribution for both raw material and acid-activated clays (S<sub>1</sub>, S<sub>2</sub> and S<sub>3</sub>) is presented in Figure 10.

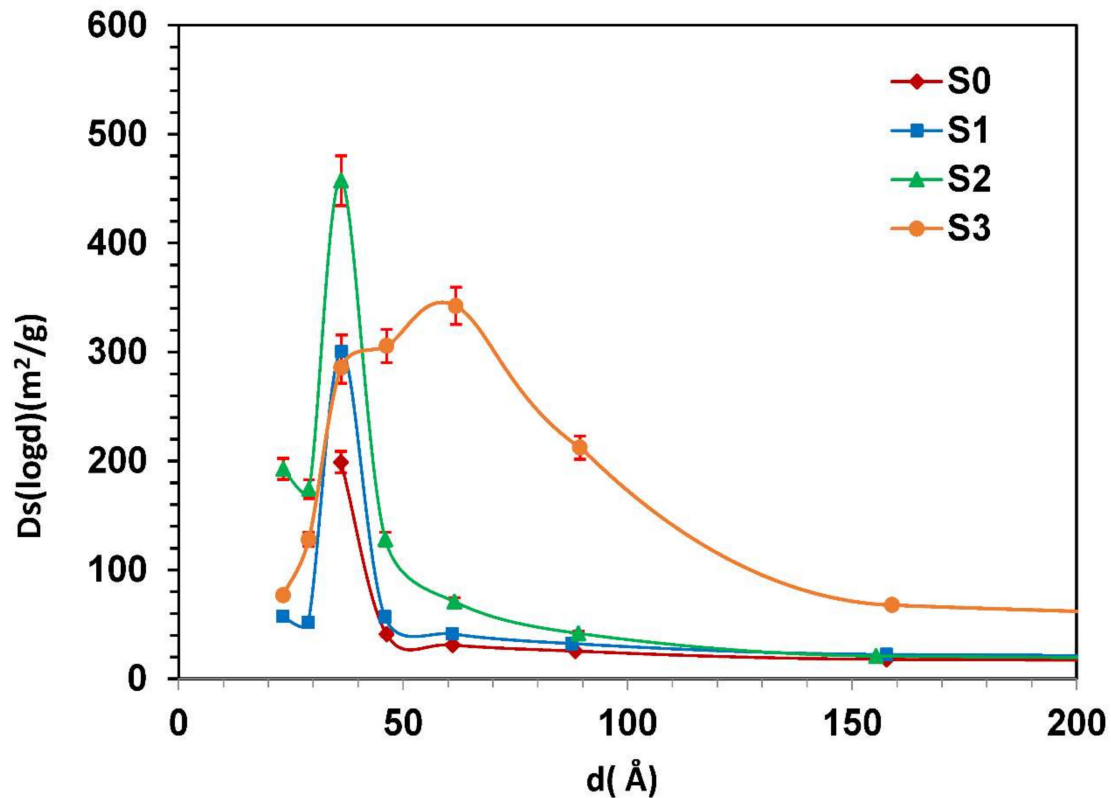


**Figure 10.** Pore size distribution curves of the raw material (S<sub>0</sub>) and activated clays (S<sub>1</sub>, S<sub>2</sub>, S<sub>3</sub>) with ±5% error bars.

From pore size analysis, it was found that the most frequent pore size of the raw material (S<sub>0</sub>) is 3.7 nm, the same result is found for samples S<sub>1</sub> and S<sub>2</sub>. However, in higher conditions, the activated clay mineral (S<sub>3</sub>) has mesopores with the most frequent size of 6 nm. The increase of peak amplitude and width of the sample S<sub>3</sub> confirm that the pore volume increases with acid-activation. The large increase in pore volume and the enlargement of the pore size distribution, observed during the strong acid treatment, suggest that significant structural changes and partial destruction may occur in this sample. Similar tendency was reported by Tatjana [9]. These changes in pore structure may result from the removal of exchangeable cations and impurities from the clay lattice following the H<sub>2</sub>SO<sub>4</sub> attack.

#### 4.5. Adsorption Equilibrium Studies of Methylene Blue (MB)

In order to evaluate the equilibrium characteristics of adsorption, three models were used to analyze the adsorption data; Langmuir; Freundlich and Frumkin models. The non-linearized forms of Langmuir, Freundlich and Frumkin models can be described by Equations (1)–(3), respectively.

$$q_e = \frac{q_{\max} K_L C_e}{1 + K_L C_e} \tag{1}$$

$$q_e = K_f C_e^{\frac{1}{n}} \tag{2}$$

$$q_e = \frac{q_{\max} K_{Fr} C_e}{\left[ e^{\left( \frac{2aq_e}{q_{\max}} \right)} + K_{Fr} C_e \right]} \tag{3}$$

where  $K_L$  (L/mg) is the Langmuir adsorption constant related to the energy of adsorption,  $q_{\max}$  and  $q_e$  (mg/g) are the maximum and equilibrium adsorption capacity, respectively.  $K_f$  and  $n$  are the Freundlich constants corresponding to adsorption capacity and intensity, respectively. For Frumkin model, the constant  $K_{Fr}$  is related to equilibrium adsorption and “ $a$ ” is the interaction parameter. A positive value of “ $a$ ” corresponds to repulsive interactions among adsorbed molecules, whereas a negative value means attraction between the adsorbed molecules. When  $a = 0$  the adsorbed molecules do not interact each other and the Frumkin isotherm reduces to Langmuir isotherm.

The adsorbed quantity of MB dye at the equilibrium ( $q_e$ ), versus residual concentration ( $C_e$ ) is presented in Figure 11.

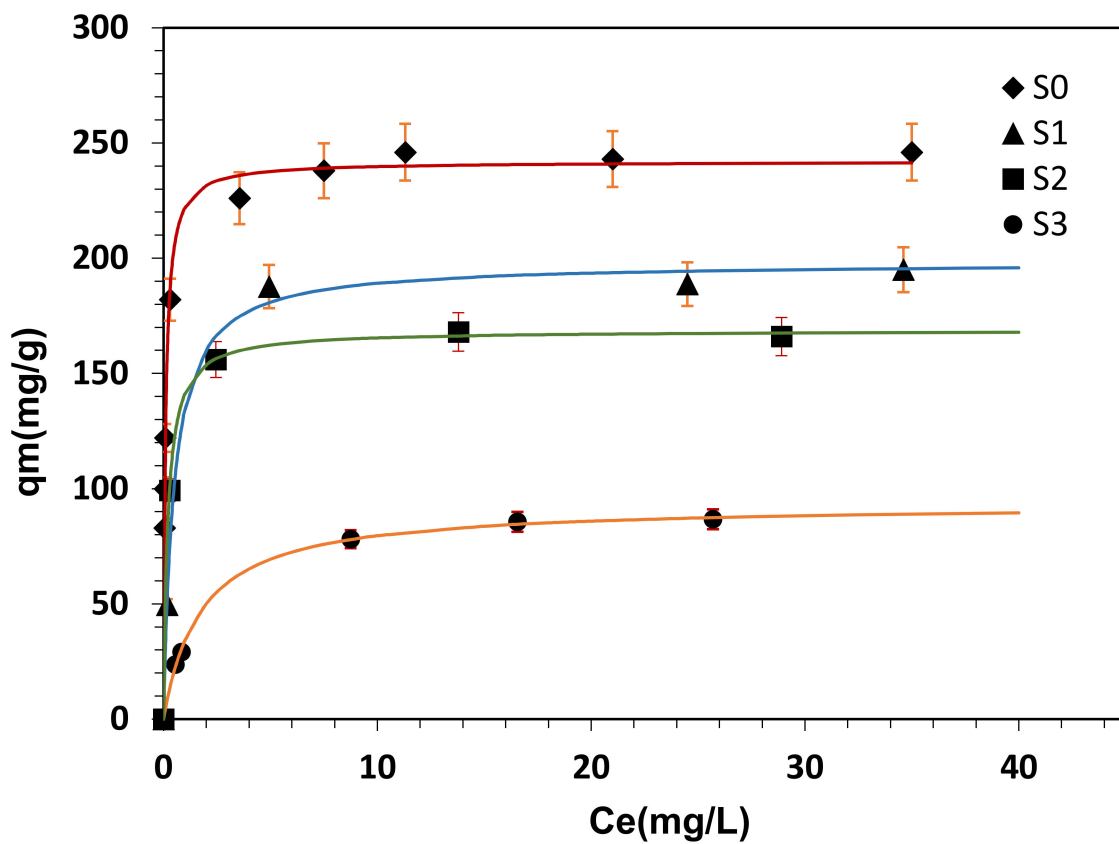


**Figure 11.** Adsorption isotherms of MB on raw material ( $S_0$ ) and activated clay samples ( $S_1$ ,  $S_2$ ,  $S_3$ ) with  $\pm 5\%$  error bars in uptake: The lines represent the fit of Langmuir model, ( $T = 20\text{ }^\circ\text{C}$ ,  $\text{pH} = 7$ ,  $m_{\text{ads}} = 200\text{ mg}$ ).

The adsorption isotherms exhibited the classical type-I behaviors of adsorbents. The Langmuir model provided the best fit to the experimental data in all range of concentrations (Figure 11). The Freundlich and Frumkin isotherms failed to correlate the results and showed large deviation (not presented). The linearization of Freundlich model ( $\ln q_e$  vs.  $\ln C_e$ ) shows a correlation factor ( $R^2$ ) of 0.87, 0.89, 0.84 and 0.97 for sample isotherms  $S_0$ ,  $S_1$ ,  $S_2$  and  $S_3$ , respectively. However the plot of equation  $\ln\left(\frac{\theta}{(1-\theta)} \frac{1}{C_e}\right)$  versus  $\theta$  for Frumkin isotherm shows linear relationship with correlation factor,  $R^2$  which did not reach 0.8 in all sample isotherms;  $S_0$ ,  $S_1$ ,  $S_2$  and  $S_3$  ( $\theta = \frac{q_e}{q_{\max}}$  represent the degree of surface coverage by the adsorbent).

The adsorption data were compared with the adsorption isotherm model of Langmuir and the parameters were estimated with regression by minimizing the sum of squared residuals. The fitting function  $\delta q$  to be minimized is established in the following equation:

$$\delta q = \sum_{i=1}^N \left( \frac{q_{\text{exp}} - q_{\text{cal}}}{q_{\text{exp}}} \right)^2 \quad (4)$$

$q_{\text{exp}}$  and  $q_{\text{cal}}$  are the experimental and the calculated adsorbed quantities at concentration  $C_e$ , respectively.  $\delta q$  is an objective function and has a relative value that depends on the fitting model and the experimental data. The deviations between the fitting model and the experimental data were determined by Equation (4),  $N$  is the number of experimental points.

$$\Delta q(\%) = \frac{100}{N} \sum_{i=1}^N \left( \frac{q_{\text{exp}} - q_{\text{cal}}}{q_{\text{exp}}} \right) \quad (5)$$

For Langmuir model, the overall mean deviation calculated by Equation (4) was <2%. The results of this analysis are illustrated in Table 3.

**Table 3.** Estimated parameter values of the Langmuir model for the raw material ( $S_0$ ) and acid-activated clay samples ( $S_1, S_2, S_3$ ).

Samples	Langmuir Constants			
	$q_{\text{max}}$ (mg/g)	$K_L$ (L/mg)	$\delta q$	$\Delta q$ (%)
$S_0$	241.91	11.019	$9.77 \times 10^{-3}$	2.63
$S_1$	198.36	2.096	$2.29 \times 10^{-3}$	1.82
$S_2$	168.59	5.115	$0.19 \times 10^{-3}$	0.13
$S_3$	93.42	0.577	$5.00 \times 10^{-3}$	2.42

Much research has reported that MB adsorption on montmorillonite, phosphorous rock and palygorskite correlate well with the Langmuir isotherm and provided a good fit with the experimental data than other isotherms [42–45]. As expected, the result suggests that the MB adsorption process by clay minerals was a single layer adsorption and that the maximum monolayer adsorption capacities were found to be 241.96, 198.36, 168.59 and 93.42 mg/g, for  $S_0, S_1, S_2$  and  $S_3$ , respectively. It is observed that the maximum quantity of MB adsorbed on raw material ( $S_0$ ) was reduced by about 60% for sample activated by strong conditions ( $S_3$ ).

The uptake of methylene blue by clays is strongly related to cationic exchange. As reported by Li et al. [46] a complete balance between MB adsorbed and desorbed exchanged cations is needed to account for the mechanism of cationic exchange. Therefore the uptake of MB is accompanied by dual mechanism of ion exchange as well as adsorption. Overall, the quantities of desorbed exchangeable cations are linearly proportional to those of adsorbed MB [45]. Moreover, the decrease in adsorption ability of MB for activated samples ( $S_1, S_2$  and  $S_3$ ) could be a consequence of the collapse of the clay lattice to some extent of acid activation. A similar result was found by Zhansheng et al. [18]; when more concentrated acids were used, the crystallinity of the clay minerals deteriorated. The decrease in MB uptake could also be attributed to the electrostatic repulsion between the positively charged surface of acid activated clays and the positively charged dye molecule in the acidic medium, in addition to the competitive adsorption between the  $H^+$  ions and dye cations to reach the surface.

## 5. Conclusions

This paper deals with the acid activation of clay minerals. It is concluded that a deep interlayer modification occurs even at low percentage of  $H_2SO_4$ . Spectroscopy analysis by infra-red (IR),

X-ray diffraction (XRD) and chemical analysis have shown that chemical structure of clay changes from a partially crystallized state to amorphous silica state at a great extent of acid-activation. This result was confirmed by the disappearance of the interstratified phase illite/smectite, which leads almost to a total destruction of natural clay structure. During acid-activation, a part of octahedral cations (magnesium, iron, aluminum) was dissolved, creating new acid sites and the interlayer exchangeable cations are replaced by protons. The content of three oxides  $\text{Al}_2\text{O}_3$ ,  $\text{Fe}_2\text{O}_3$  and  $\text{MgO}$  of the raw material decreased from 14.27; 6.07; 1.46 to 9.4%; 1.89%; 0.43% for severe acid-treatment ( $\text{S}_3$ ), respectively. Acid attack process mainly affected the smectite phase of clay and caused a broad pore distribution of material, created mesopores and increased external surface area of clay. Acid-activation of clay minerals reduces the adsorption capacity of methylene blue used as cationic dye; this is attributed to the competition between the  $\text{H}^+$  ions and dye cations to reach the surface. Also, this clear decrease could be a consequence of the partial collapse of the clay lattice to some extent of acid activation.

**Author Contributions:** A.A. conceived, designed and performed the experiments and wrote the first draft of the manuscript; H.G. and M.I.K. analysed the data and revised the manuscript; M.K.A. and A.M.E. revised the interpretation of the data and contributed to the revision of the manuscript; A.G. supervised the research work.

**Funding:** This research was funded by King Khalid University, Abha-KSA.

**Acknowledgments:** The authors extend their appreciation to the Deanship of Scientific Research at King Khalid University, Abha-KSA, for funding this work through General Research Project under grant number (G.R.P-358-38).

**Conflicts of Interest:** The authors declare no conflict of interest.

## References

1. Fonseca, C.G.; Vaiss, V.S.; Wypych, F.; Diniz, R.; Leitão, A.A. Investigation of the initial stages of the montmorillonite acid-activation process using DFT calculations. *Appl. Clay Sci.* **2018**, *165*, 170–178. [[CrossRef](#)]
2. Arus, V.A.; Nousir, S.; Sennour, R.; Shiao, T.Z.; Nistor, I.D.; Roy, R.; Azzouz, A. Intrinsic affinity of acid-activated bentonite towards hydrogen and carbon dioxide. *Int. J. Hydrogen Energy* **2018**, *43*, 7964–7972. [[CrossRef](#)]
3. Vryzas, Z.; Kelessidis, V.C.; Nalbantian, L.; Zaspalis, V.; Gerogiorgis, D.I.; Wubuliksimu, Y. Effect of temperature on the rheological properties of neat aqueous Wyoming sodium bentonite dispersions. *Appl. Clay Sci.* **2017**, *136*, 26–36. [[CrossRef](#)]
4. Bouazizi, A.; Saja, S.; Achiou, B.; Ouammou, M.; Calvo, J.I.; Aaddane, A.; Younsi, S.A. Elaboration and characterization of a new flat ceramic MF membrane made from natural Moroccan bentonite. Application to treatment of industrial wastewater. *Appl. Clay Sci.* **2016**, *133*, 33–40. [[CrossRef](#)]
5. Garshasbi, V.; Jahangiri, M.; Anbia, M. Equilibrium  $\text{CO}_2$  adsorption on zeolite 13X prepared from natural clays. *Appl. Clay Sci.* **2017**, *393*, 225–233.
6. Elmoubarki, R.; Mahjoubi, F.Z.; Tounsadi, H.; Moustadrafa, J.; Abdennouri, M.; Zouhri, A.; El Albani, A.; Barka, N. Adsorption of textile dyes on raw and decanted Moroccan clays: Kinetics, equilibrium and thermodynamics. *Water Resour. Ind.* **2015**, *9*, 16–29. [[CrossRef](#)]
7. Carrado, K.A.; Komadel, P. Acid Activation of Bentonites and Polymer-Clay Nanocomposites. *Elements* **2009**, *5*, 111–116. [[CrossRef](#)]
8. Zhua, J.; Zhanga, P.; Wang, Y.; Wena, K.; Sua, X.; Zhua, R.; Hea, H.; Xie, Y. Effect of acid activation of palygorskite on their toluene adsorption behaviors. *Appl. Clay Sci.* **2018**, *159*, 60–67. [[CrossRef](#)]
9. Novakovic, T.; Rozic, L.; Petrovic, S.; Rosic, A. Synthesis and characterization of acid-activated Serbian smectite clays obtained by statistically designed experiments. *Chem. Eng. J.* **2008**, *37*, 436–442. [[CrossRef](#)]
10. Javed, S.H.; Zahir, A.; Khan, A.; Afzal, S.; Mansha, M. Adsorption of Mordant Red 73 dye on acid activated bentonite: Kinetics and thermodynamic study. *J. Mol. Liq.* **2018**, *254*, 398–405. [[CrossRef](#)]
11. Liu, Y.; Gates, W.P.; Bouazza, A. Acid induced degradation of the bentonite component used in geosynthetic clay liners. *Geotext. Geomembr.* **2013**, *36*, 71–80. [[CrossRef](#)]

12. Gannouni, A.; Bellagi, A.; Bagane, M. Preparation of activated clay for the bleaching of olive oil. *Ann. Chim. Sci. Mat.* **1999**, *24*, 407–416. [[CrossRef](#)]
13. Komadel, P.; Madejova, J. Acid Activation of Clay Minerals. In *Handbook of Clay Science*; Bergaya, F., Theng, B.K.G., Lagaly, G., Eds.; Elsevier Science: Amsterdam, The Netherlands, 2006; pp. 263–287.
14. Jedli, H.; Brahmi, J.; Hedfi, H.; Mbarek, M.; Bouzgarrou, S.; Slimi, K. Adsorption kinetics and thermodynamics properties of Supercritical CO<sub>2</sub> on activated clay. *J. Pet. Sci. Eng.* **2018**, *166*, 476–481. [[CrossRef](#)]
15. Amari, A.; Chlendi, M.; Gannouni, A.; Bellagi, A. Experimental and theoretical studies of VOC adsorption on acid-activated bentonite in a fixed-bed adsorber. *Ind. Eng. Chem. Res.* **2010**, *49*, 11587–11593. [[CrossRef](#)]
16. Moraes, D.S.; Miranda, L.C.R.; Angélica, R.S.; Filho, G.N.R.; Zamian, J.R. Functionalization of bentonite and vermiculite after the creation of structural defects through an acid leaching process. *J. Braz. Chem. Soc.* **2018**, *29*, 320–327. [[CrossRef](#)]
17. Sidorenko, A.Y.; Kravtsova, A.V.; Aho, A.; Heinmaa, I.; Kuznetsov, T.F.; Murzin, D.Y.; Agabekova, V.E. Catalytic isomerization of  $\alpha$ -pineneoxide in the presence of acid-modified clays. *J. Mol. Catal.* **2018**, *448*, 18–29. [[CrossRef](#)]
18. Zhansheng, W.U.; Chun, L.I.; Xifang, S.; Xiaolin, X.; Bin, D.; Jine, L.; Hongsheng, Z. Characterization, acid activation and bleaching performance of bentonite from Xinjiang. *Chin. J. Chem. Eng.* **2006**, *14*, 253–258.
19. Anirudhan, T.S.; Ramachandran, M. Adsorptive removal of basic dyes from aqueous solutions by surfactant modified bentonite clay (organo clay): Kinetic and competitive adsorption isotherm. *Process Saf. Environ. Prot.* **2015**, *95*, 215–225. [[CrossRef](#)]
20. Yan, Z.; Fu, L.; Yang, H.; Ouyang, J. Amino-functionalized hierarchical porous SiO<sub>2</sub>-AlOOH composite nanosheets with enhanced adsorption performance. *J. Hazard. Mater.* **2018**, *344*, 1090–1100. [[CrossRef](#)] [[PubMed](#)]
21. Bergaya, F.; Lagaly, G. Surface modification of clay minerals. *Appl. Clay Sci.* **2001**, *19*, 1–3. [[CrossRef](#)]
22. Bergaya, F.; Theng, B.K.G.; Lagaly, G. Modified Clays and Clay Minerals. In *Handbook of Clay Science*; Bergaya, F., Theng, B.K.G., Lagaly, G., Eds.; Elsevier Science: Amsterdam, The Netherlands, 2006; pp. 261–262.
23. Hart, M.P.; Brown, D.R. Surface acidities and catalytic activities of acid-activated clays. *J. Mol. Catal. A Chem.* **2004**, *212*, 315–321. [[CrossRef](#)]
24. Mikhail, S.; Zaki, T.; Khalil, L. Desulfurization by an economically adsorption technique. *Appl. Catal. A* **2002**, *227*, 265–278. [[CrossRef](#)]
25. Taylor, D.R.; Jenkins, D.B.; Ungermann, C.B. Bleaching with alternative layered minerals: A comparison with acid activated montmorillonite for bleaching soybean. *J. Am. Oil Chem. Soc.* **1989**, *66*, 334–341. [[CrossRef](#)]
26. Rhodes, C.N.; Brown, D.R. Structural characterization and optimization of acid-treated montmorillonite and high-porosity silica supports for ZnCl<sub>2</sub> alkylation catalysts. *J. Chem. Soc. Faraday Trans.* **1992**, *88*, 2269–2274. [[CrossRef](#)]
27. Komadel, P. Chemically modified smectites. *Clay Miner.* **2003**, *38*, 127–138. [[CrossRef](#)]
28. Mokaya, R.; Jones, W. Pillared clays and pillared acid-activated Clays: A comparative study of physical, acidic, and catalytic properties. *J. Catal.* **1995**, *53*, 76–85. [[CrossRef](#)]
29. Pardo, L.; Cecilia, J.A.; Moreno, C.L.; Hernández, V.; Pozo, M.; Bentabol, M.J.; Franco, F. Influence of the Structure and Experimental Surfaces Modifications of 2:1 Clay Minerals on the Adsorption Properties of Methylene Blue. *Minerals* **2018**, *8*, 359. [[CrossRef](#)]
30. Şahin, O.; Kaya, M.; Saka, C. Plasma-surface modification on bentonite clay to improve the performance of adsorption of methylene blue. *Appl. Clay Sci.* **2015**, *116–117*, 46–53. [[CrossRef](#)]
31. Guerra, D.J.L.; Mello, I.; Freitas, L.R.; Resende, R.; Silva, R.A.R. Equilibrium, thermodynamic, and kinetic of Cr (VI) adsorption using a modified and unmodified bentonite clay. *Int. J. Min. Sci. Technol.* **2014**, *24*, 525–535. [[CrossRef](#)]
32. Hu, P.; Wang, J.; Huang, R. Simultaneous removal of Cr(VI) and Amido black 10B (AB10B) from aqueous solutions using quaternized chitosan coated bentonite. *Int. J. Biol. Macromol.* **2016**, *92*, 694–701. [[CrossRef](#)] [[PubMed](#)]
33. Brown, G.; Brindley, G.W. X-Ray Diffraction Procedures for Clay Minerals Identification. In *Crystal Structures of Clay Minerals and their X-Ray Identification*; Brindley, G.W., Brown, G., Eds.; Mineralogical Society: London, UK, 1980; pp. 305–360.
34. Fiore, S.; Cuadros, J.; Huertas, F.J. *Interstratified Clay Minerals: Origin, Characterization and Geochemical Significance*; Digilabs: Bari, Italy, 2013.

35. Reynolds, R.C. Interstratified Clay Minerals. In *Handbook of Crystal Structures of Clay Minerals and Their X-ray Identification*; Brindley, G.W., Brown, G., Eds.; Mineralogical Society: London, UK, 1980; pp. 249–303.
36. Temuujin, J.; Jadambaa, T.; Burmaa, G.; Erdenechimeg, S.; Amarsanaa, J.; MacKenzie, K.J.D. Characterisation of acid activated montmorillonite clay from Tuulant (Mongolia). *Ceram. Int.* **2004**, *30*, 251–255. [[CrossRef](#)]
37. Shinoda, T.; Onaka, M.; Izumi, Y. Proposed models of mesopore structures in sulfuric acid-treated montmorillonites and K10. *Chem. Lett.* **1995**, *24*, 495–496. [[CrossRef](#)]
38. Khalil, A.A.; Abo, O.; El-Wafa, S.; Sallam, A.; ElKorashy, S.A. Characterization of some Sinai clay deposits. *Mag. Verfahrenstech.* **1988**, *12*, 396–400.
39. Sing, K.; Everet, D.; Haul, R.; Moscou, L.; Pierotti, R.; Rouquerol, J.; Siemieniewska, T. Reporting physisorption data for gas/solid systems with special reference to the determination of surface area and porosity. *Pure Appl. Chem.* **1985**, *57*, 603. [[CrossRef](#)]
40. Jovanovic, N.; Janackovic, J. Pore structure and adsorption properties of an acid-activated bentonite. *Appl. Clay Sci.* **1991**, *6*, 59–68. [[CrossRef](#)]
41. Barrett, E.P.; Joyner, L.C.; Halenda, P.P. The determination of pore volume and area distribution in porous substances. I. Computation from nitrogen isotherms. *J. Am. Chem. Soc.* **1951**, *73*, 373–380.
42. Almeida, C.A.P.; Debacher, N.A.; Downsc, A.J.; Cotteta, L.; Mello, C.A.D. Removal of methylene blue from colored effluents by adsorption on montmorillonite clay. *J. Colloid Interface Sci.* **2009**, *332*, 46–53. [[CrossRef](#)] [[PubMed](#)]
43. Al-Futaisi, A.; Jamrah, A.; Al-Hanai, R. Aspects of cationic dye molecule adsorption to palygorskite. *Desalination* **2007**, *214*, 327–342. [[CrossRef](#)]
44. Malash, G.F.; El-Khaiary, M.I. Methylene blue adsorption by the waste of Abu-Tartour phosphate rock. *J. Colloid Interface Sci.* **2010**, *348*, 537–545. [[CrossRef](#)] [[PubMed](#)]
45. Mouzdahir, Y.E.; Elmchaouri, A.; Mahboub, R.; Gil, A.; Korili, S.A. Adsorption of methylene blue from aqueous solutions on a Moroccan clay. *J. Chem. Eng. Data* **2007**, *52*, 1621–1625. [[CrossRef](#)]
46. Li, Z.; Chang, O.H.; Jiang, W.T.; Jean, J.S.; Hong, H. Mechanism of methylene blue removal from water by swelling clays. *Chem. Eng. J.* **2011**, *168*, 1193–1200. [[CrossRef](#)]



© 2018 by the authors. Licensee MDPI, Basel, Switzerland. This article is an open access article distributed under the terms and conditions of the Creative Commons Attribution (CC BY) license (<http://creativecommons.org/licenses/by/4.0/>).